Phonon softening and the phase transition in VN

V. I. Ivashchenko[1] and P. E. A. Turchi[2]
[1]*Institute of Problems of Materials Science, NAS of Ukraine, Krzhyzhanovsky Street 3, 03142 Kyiv, Ukraine*
[2]*Lawrence Livermore National Laboratory (L-352), P.O. Box 808, Livermore, California 94551, USA*
(Received 16 September 2008; published 31 December 2008)

Based on an analysis of phonon modes and the results of first-principles total-energy calculations for the cubic, tetragonal, and orthorhombic phases of VN, a possible mechanism of the cubic (space group $Fm\bar{3}m$) to tetragonal (space group $P\bar{4}2m$) phase transition at 205 K is proposed. The mechanism suggests that spontaneous volume and shear strains, $e_A=\varepsilon_{xx}+\varepsilon_{yy}+\varepsilon_{zz}$ and $e_{E1}=2\varepsilon_{zz}-\varepsilon_{xx}-\varepsilon_{yy}$, are induced indirectly by the collapse of the X_3' mode, indicating that the tetragonal phase exhibits improper ferroelasticity. The effect of nonmetal vacancy composition on phase transition is also discussed.

DOI: 10.1103/PhysRevB.78.224113 PACS number(s): 64.60.Ej, 63.20.dk, 71.15.Nc, 71.20.−b

I. INTRODUCTION

Vanadium nitride (VN) crystallizes with a NaCl-type structure and exhibits properties inherent to refractory transition-metal compounds.[1,2] Its high melting temperature (2050 °C), electrical conductivity $[(60-127)\times10^{-6}\ \Omega\ \mathrm{cm}]$, and chemical stability at high nitrogen composition (VN_x, $0.7\leq x\leq1.0$) suggest that the V-N and V-V bonds are very strong and covalent in nature, as confirmed by band-structure calculations for VN (Refs. 2 and 3) and VN_x.[4] It was established that, in VN_x, the ordering of nitrogen vacancies takes place in the range of $VN_{0.74}$–$VN_{0.84}$ below 793 K.[5] The vacancy arrangement has tetragonal symmetry; however, the metal sublattice is cubic within the experimental accuracy.[5] A review of the electronic structure properties and the lattice dynamics of transition-metal carbides and nitrides has been given in Ref. 6. The most interesting peculiarity of this compound is the cubic-to-tetragonal structural transformation at 205 K,[7] the mechanism of which is still unknown. This mechanism should account for the following main peculiarities of this phase transition.[7]

(a) $VN_{0.99}$, space group $Fm\bar{3}m$, transforms at 205 K into a tetragonal noncentrosymmetric low-temperature modification with space group $P\bar{4}2m$.

(b) The phase transition is presumably due to an electronic instability that leads to a clustering of the metal atoms into tetrahedral units.

(c) The structural changes extend in the tetragonal low-temperature modification: at 20 K a triclinic lattice consistent with tetragonal symmetry was identified.

(d) At the transition point a jump in the heat capacity was observed.

(e) $VN_{0.97}$ shows no evidence of the phase transition in both x-ray diffraction (XRD) and heat-capacity measurements.

(e) The symmetry of the low-temperature structure ($P\bar{4}2m$) compared to that of the high-temperature structure ($Fm\bar{3}m$) suggests a first-order phase transition. The expected discontinuity in the cell volume for such a transition is less than 0.1 $\mathrm{Å}^3$ (however, this point needs to be clarified).

(f) In VN_x, phonon anomalies in the acoustic branch at the X point were observed by inelastic neutron-diffraction measurements.[8]

(g) At room temperature the mean-square displacement amplitude of the metal atoms, $\langle u^2\rangle_V=0.006$ Å^2, is much larger than that of the nonmetal atoms ($\langle u^2\rangle_N=0.004$ Å^2). The ratio $\langle u^2\rangle_V/\langle u^2\rangle_N$ of about 0.91 at 20 K increases to 1.41 at room temperature.

In the present investigation we propose a possible mechanism of phase transformation in VN_x that is able to account for most of the above-mentioned peculiarities. Our findings suggest that spontaneous volume and shear strains are induced in the tetragonal phase as a result of an indirect coupling of the X_3, mode to homogeneous elastic strains. This mechanism follows from the results of first-principles calculations of the electronic structure and phonon properties of the cubic, tetragonal, and orthorhombic modifications of vanadium nitrides. The investigations were carried out using a combined first-principles pseudopotential (PP) approach and full-potential linearized augmented plane-wave (FLAPW) method. The paper is organized as follows. In Sec. II we present our theoretical framework and the computational details. Section III contains the results of calculations and their interpretation. Finally, the main conclusions are presented in Sec. IV.

II. DETAILS OF FIRST-PRINCIPLES CALCULATIONS

Two first-principles procedures, namely, the PP approach and FLAPW method, were employed to investigate the cubic, tetragonal, and orthorhombic structures of VN and the simple cubic (SC) ($Pm3m$) and body-centered-tetragonal (bct) ($I4/mmm$) structures of $VN_{0.75}$. The bct structure was selected since it represents an appropriate approximation of the ordered phases for $VN_{0.74–0.84}$.[5] The lattice constant of the latter phases is twice as large as that of the original fcc VN. Therefore we could not calculate these structures because of the large number of the atoms inside the cubic unit cell (larger than 58 atoms). Scalar-relativistic band-structure calculations within the local-density approximation (LDA) of density-functional theory (DFT) were carried out for an eight atom supercell of V_4N_4 (VN) and for a seven-atom supercell of V_4N_3 ($VN_{0.75}$). The QUANTUM-ESPRESSO first-principles code[9] was used to perform the PP calculations with Vanderbilt ultrasoft pseudopotentials to describe the electron-ion interaction.[10] In the Vanderbilt approach,[10] the orbitals are

allowed to be as soft as possible in the core regions so that their plane-wave expansion converges rapidly. The semicore states were treated as valence states. For the vanadium pseudopotential, the nonlinear core corrections were taken into account.[9] Plane waves up to a kinetic-energy cutoff of 38 Ry were included in the basis set. The exchange-correlation potential was treated in the framework of the generalized gradient approximation (GGA) of Perdew-Burke-Ernzerhof.[11] Brillouin-zone (BZ) integrations have been performed using sets of special points corresponding to the (8 8 8) Monkhorst-Park nonshifted mesh.[12] Each eigenvalue was convoluted with a Gaussian with different widths, σ, in the energy range of 0.01–0.16 Ry. The Broyden method[13] was used for the simultaneous relaxation of the ions and the unit cell while the symmetry was preserved. The relaxation of the atomic coordinates and of the unit cell was considered to be complete when the atomic forces were less than 0.05 mRy/bohr, the stresses were smaller than 10 MPa, and the variation in the total energy during the structural optimization iterative process was less than 0.05 mRy.

The above-described PP procedure was employed to study the phonon spectra of cubic and tetragonal VN and $VN_{0.75}$ in the framework of the density-functional perturbation theory (DFPT) described in Refs. 9 and 14. For fcc-based VN, integrations over the BZ were carried out using the (12 12 12) mesh of k points, and the phonon spectra were computed with a (8 8 8) q mesh for various smearing parameters σ. In the case of the bct $VN_{0.75}$ phase, the BZ integration was done using the (8 8 4) mesh of k points. The phonon frequencies for the $VN_{0.75}$ structures were computed with a (2 2 2) q mesh for σ=0.02 Ry. For both the stoichiometric and substoichiometric compounds, the computed phonon frequencies were interpolated on a (16 16 16) q mesh to correctly calculate the phonon density of states (PDOS) using the tetrahedron method.[9] Another approach to lattice dynamics, the so-called direct supercell method that was applied to VN, is based on the force calculations via the Hellmann-Feynman theorem in the total-energy calculations.[15] The force-constant matrices are derived from atomic forces. We have employed the computational code PHON (Ref. 16) that requires the atomic forces as input information. We considered the (2 2 2) fcc supercell, in which case the phonon frequencies are exact at the Γ, X, and L points. The atomic forces were calculated with the PP method and a (4 4 4) mesh of k points. Two independent runs of force fields have been carried out: one for V and one for N atoms, all displaced by (0.005 0.005 0.005)a, where a is the lattice parameter.

The FLAPW method as implemented in the WIEN97 code[17,18] was used to optimize the tetragonal structure of VN. The "muffin-tin" radii were 2.00 and 1.75 bohr for V and N atoms, respectively. The maximum number of plane waves is determined by the parameter $R_{mt}K_{max}$, which was 8 [R_{mt} is the radius of the smallest atomic spheres and K_{max} is the largest reciprocal wave vector used in the linearized augmented plane-wave (LAPW) basis set]. The semicore states were considered as valence states, while the core states were treated as atomiclike states. To describe the exchange-correlation energy, the GGA (Ref. 11) was considered. The criterion of convergence for the total energy was 0.1 mRy. Integration over the BZ was performed using the (8 8 8) and (4 4 4) meshes of k points for the fcc and primitive tetragonal cells, respectively. A three-step relaxation procedure was used to optimize atomic positions, c/a ratio, and cell volume. It was assumed that the relaxation of the free-atomic coordinates was achieved when the atomic forces were less than 1 mRy/bohr.

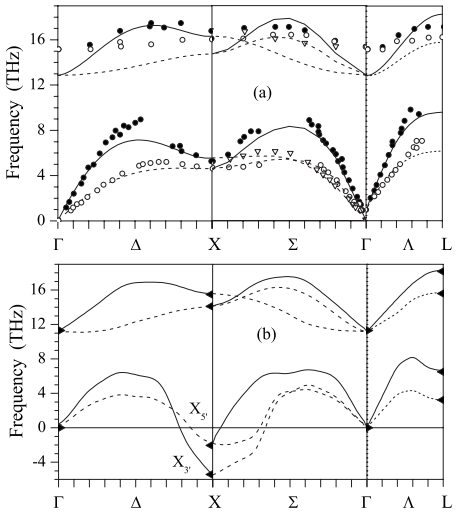

FIG. 1. (a) Experimental phonon-dispersion curves along high-symmetry directions for $VN_{0.86}$ (Ref. 8). Full circles and open triangles and circles refer to longitudinal and transverse modes, respectively. Longitudinal (full line) and transverse (dashed line) phonon frequencies for VN calculated for (a) σ=0.12 Ry and (b) σ=0.03 Ry. Full triangles are the corresponding frequencies determined using the (b) supercell direct method. "Negative" frequencies actually mean "imaginary" (negative squared frequencies). The labels given to the acoustic modes at the X point are compatible with those given in Refs. 19 and 20.

III. RESULTS AND DISCUSSION

In Fig. 1, the phonon-dispersion curves for substoichiometric $VN_{0.86}$ derived from inelastic neutron-scattering measurements[8] are shown. A pronounced softening of the acoustic modes near the X point is observed. The semiempirical tight-binding calculations of the phonon spectrum for stoichiometric VN allowed Weber *et al.*[8] to establish a plausible origin of the observed phonon softening. In VN, the Fermi level (E_F) lies near a twofold-degenerate $W_{3'}$ level (not shown here), and the electronic transitions at the Fermi surface between two $W_{3'}$ states at the W $2\pi/a$ (0, 1, 1/2) and $2\pi/a$ (0, 1, −1/2) points strongly increase a negative contribution to the dynamics matrix for the phonon wave vector X, $2\pi/a$ (0, 0, 1).[8] A very deep phonon softening compared to experiment was obtained, and only the introduction of nitrogen vacancies led to a better agreement with experiment.

To account for the effects of temperature and nitrogen vacancies on the phonon spectrum of VN_x we first calculated the phonon-dispersion curves by using various values of band-energy smearing σ. The motivation for such an approach is as follows. The Korringa-Kohn-Rostoker-coherent-potential-approximation (KKR-CPA) energy-band calculations of VN_x (Ref. 4) showed that at small vacancy

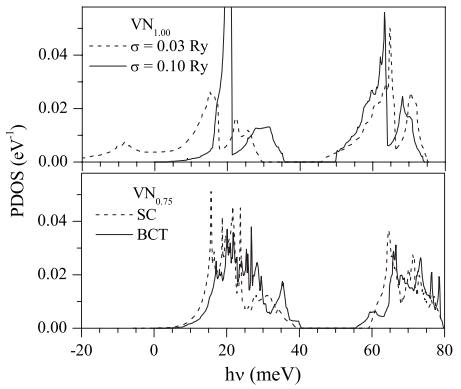

FIG. 2. PDOSs for $VN_{1.0}$ calculated at σ=0.03 and 0.10 Ry (dashed and solid lines, respectively) and PDOS of the SC and bct of $VN_{0.75}$ (dashed and solid line, respectively).

compositions $(1-x<0.1)$ the dangling-bond states are located in a minimum of the density of states (DOS), below E_F, and the main effect of disordering on the band energies around E_F was a band smearing and a lowering of the Fermi level. It is also well known that, to a first approximation, temperature effect results in a smearing of the band energies. In order to substantiate the hypothesis of an acoustic-mode softening around the X point that occurs upon a decrease in temperature and an increase in nitrogen composition, x, in VN_x, we calculated the phonon-dispersion curves along high-symmetry lines for several values of the smearing parameter σ using the DFPT. These phonon spectra are displayed in Fig. 1. We note that the calculated dispersion curves for stoichiometric VN (σ=0.03 Ry) are characterized by a pronounced phonon softening of the acoustic branch at the X point. An increase in σ, which implies an increase in temperature and nitrogen vacancies, leads to the disappearance of the phonon anomalies and a better agreement between calculated and experimental spectra [cf. Fig. 1(a)]. This finding fairly validates our approximate scheme. Moreover, to make sure that the phonon anomalies are not a consequence of the accepted conditions of the PP calculations, the phonon frequencies were calculated by using another approach, namely, the direct supercell method.[15,16] The results presented in Fig. 1(b) show that both approaches confirm the existence of phonon anomalies. Furthermore, our dispersive curves for VN were compared with those obtained by the method proposed by Isaev *et al.*,[6] and an excellent agreement between the two results was found.

We also employed the DFPT to calculate the PDOS for both the SC- and bct-ordered $VN_{0.75}$. After structural optimization the structural parameters were a=4.063 Å (SC), a =4.068 Å, and c/a=2 (bct). In the bct structure, the vacancy arrangement has tetragonal symmetry, and the metal atoms located in the neighborhood of a vacancy shift from their standard positions by 0.037 Å. The total energy of the latter structure was found to be lower than that of the SC structure by 22 mRy/cell. In Fig. 2, we show the calculated phonon densities of states for VN_x. An increase in σ leads to a noticeable shift in the acoustic PDOS toward high frequencies. The PDOSs of $VN_{0.75}$ are more structured compared to those of VN due to the vacancy superstructure. The ranges of

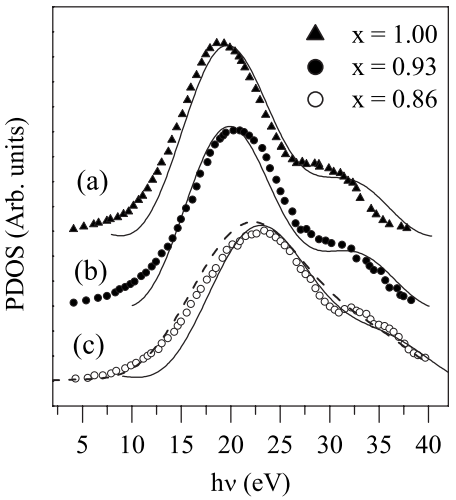

FIG. 3. Experimental PDOSs for VN_x (Ref. 8) (scatters) calculated PDOS for VN at (a) σ=0.10, (b) 0.12, and (c) 0.16 Ry (solid lines) and calculated PDOS for bct (c) $VN_{0.75}$ (dashed line).

acoustic frequencies in $VN_{0.75}$ and VN computed at large σ almost coincide, whereas the optical branch in VN is lower compared to that in $VN_{0.75}$. In order to correctly compare the calculated and experimental PDOSs, we averaged the calculated PDOSs over 50 points to account for the observed phonon width.[8] A comparison of the experimental and theoretical phonon spectra is presented in Fig. 3. In the experimental spectra, the expected van Hove singularities are washed out. This indicates that the large phonon linewidths observed in VN_x probably persist as one approaches the stoichiometric compound. For increasing x a pronounced softening is observed. It is seen also that an increase in σ has the same effect on the phonon density of states as a decrease of x in VN_x. A good agreement between the calculated PDOS for $VN_{0.75}$ and the experimental PDOS for $VN_{0.86}$ is observed. We note that the PDOSs for $VN_{0.75}$ and VN computed at large σ do not show any soft modes.

We already stressed the key role of the electronic transitions between the $W_{3'}$ states being responsible for the phonon anomalies in the acoustic branch at the X point. The closer the Fermi level is to the energy of $W_{3'}$ states, the dipper the phonon anomalies are. In Fig. 4, we show the effect of the band-energy smearing, σ, on the position of E_F

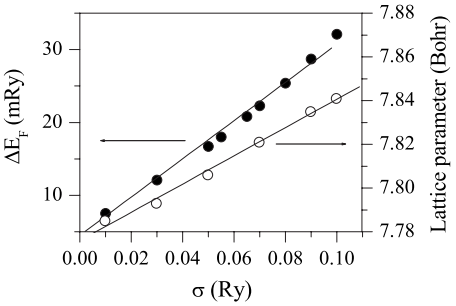

FIG. 4. Energy difference $\Delta E_F=E(W_{3'})-E_F$ and lattice parameter for the $Fm\bar{3}m$ phase as functions of σ. Here and in the following figures the line is a polynomial fit to the data points (to be considered as a guide for the eyes).

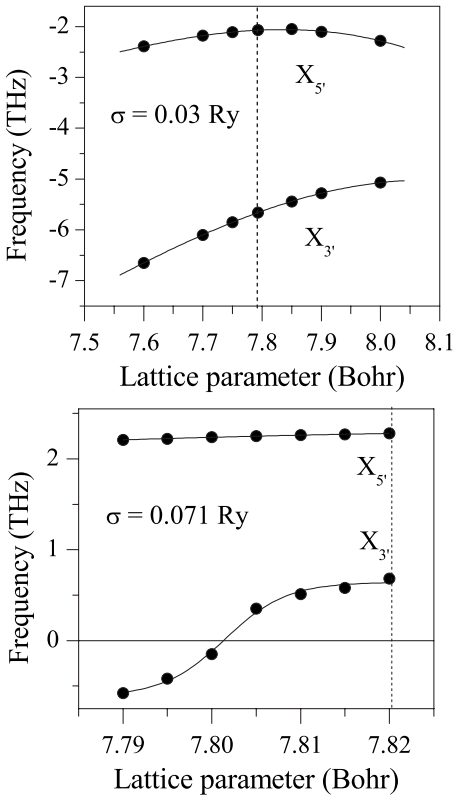

FIG. 5. Frequencies of the $X_{3'}$ and $X_{5'}$ acoustic phonons in the $Fm\bar{3}m$ phases computed at σ=0.03 and 0.071 Ry as functions of the lattice parameter. The vertical line denotes the equilibrium lattice parameter for a given value of σ.

with respect to the $W_{3'}$ level. The Fermi level gradually moves away from the $W_{3'}$ level as σ increases. As a result, the frequencies of both the soft $X_{3'}$ (X_4 in the notation of Ref. 9) and $X_{5'}$ acoustic phonons increase. This finding explains to a large extent why an increase in temperature or vacancy composition leads to a decrease in the phonon anomalies in VN_x.[8]

In Fig. 4, we also present the equilibrium lattice parameter as a function of σ. It is seen that the lattice parameter increases with the band-energy smearing. Therefore it is concluded that a reduction in the lattice constant could enhance the phonon softening. To verify this hypothesis we investigated the change in soft phonon frequencies with lattice parameter at fixed values of σ. The frequencies of the acoustic soft modes as functions of the lattice parameter are shown in Fig. 5. We see that a change in lattice parameter a has a noticeable effect on the soft modes for the structure computed at σ=0.071 Ry. It will be shown below, for this particular value of σ, that a phase transition takes place. Further reduction in σ (that automatically leads to reducing a, for example, during cooling) gives rise to phonon softening. Since a change in σ implies a corresponding change in the lattice parameter (cf. Fig. 4), we note that the band-energy smearing is a more appropriate parameter than the lattice parameter. Below we will further examine the changes in the electronic and phonon structures with σ.

The collapse of the acoustic $X_{3'}$ mode causes the phase transition, whose order parameter is the amplitude of the atomic displacements along the phonon normal coordinates. The small group of the X point is D_{4h}, and the star of the X point is made of three equivalent points $\mathbf{k}_1=(2\pi/a,0,0)$, $\mathbf{k}_2=(0,2\pi/a,0)$, and $\mathbf{k}_3=(0,0,2\pi/a)$. The amplitudes of the normal coordinates related to $\mathbf{k}_1$, $\mathbf{k}_2$, and $\mathbf{k}_3$ vectors are Q_1, Q_2, and Q_3, respectively. The $X_{3'}$ irreducible representation is not degenerate, so the order parameter Q associated with the soft mode is three dimensions. Group-theoretical considerations considerably restrict the number of possible low-symmetry phases that can arise after the collapse of the acoustic $X_{3'}$ mode. There are six possible crystal structures corresponding to a different direction in the three-dimensional space of the order parameter.[19,20] Following the notation in Ref. 20, these structures can be classified as in Table I. We will focus on the $C2$ line whose symmetry is compatible with the observed x-ray diffraction pattern of the low-temperature phase.[7] In addition, we included in the list of possible phases the initial cubic phase $P0$ ($Fm\bar{3}m$) to make the structural analysis more general. Below we will follow the phase notation presented in Table I.

TABLE I. Classification of the possible stable phases along particular directions (the order-parameter space, $\mathbf{Q}$) (Ref. 20). Q_1, Q_2, and Q_3 are the amplitudes of the normal coordinates of the X_3' mode that are characterized by the wave vectors $\mathbf{k}_1=(2\pi/a,0,0)$, $\mathbf{k}_2=(0,2\pi/a,0)$, and $\mathbf{k}_3=(0,0,2\pi/a)$, respectively.

Direction, $\mathbf{Q}$	Configuration	No. of space group	Space group	Structure
$P0$	(0,0,0)	225	$Fm\bar{3}m$	Cubic
$P1$	$(Q_1,0,0)$	129	$P4/nmm$	Tetragonal
$P2$	$(Q_1,Q_1,0)$	132	$P4_2/mcm$	Tetragonal
$P3$	(Q_1,Q_1,Q_1)	215	$P\bar{4}3m$	Cubic
$C1$	$(Q_1,Q_2,0)$	49	$Pccm$	Orthorhombic
$C2$	(Q_1,Q_1,Q_2)	111	$P\bar{4}2m$	Tetragonal
$S1$	(Q_1,Q_2,Q_3)	16	$P222$	Orthorhombic

When the acoustic $X_{3'}$ mode softens, spontaneous elastic strains can be induced through the coupling between the atomic displacements that correspond to one of the six directions (cf. Table I) and the macroscopic strains, i.e., between zone-center and zone-border acoustic phonons. The free energy that specifies the phase transition can be expressed by the following equation:

$$F = F(\mathbf{Q}) + F(\mathbf{e},\mathbf{Q}) + F(\mathbf{e}), \tag{1}$$

where $F(\mathbf{Q})$ is the free energy associated with the $X_{3'}$ mode, $F(\mathbf{e},\mathbf{Q})$ refers to the coupling between the $X_{3'}$ mode and the strains, and $F(\mathbf{e})$ corresponds to homogeneous elastic strains. The free-energy invariants under the symmetry operations of O_{5h} can be constructed[21,22] as follows:

$$F(\mathbf{Q}) = \alpha(Q_x^2+Q_y^2+Q_z^2) + \beta(Q_x^4+Q_y^4+Q_z^4) + \gamma(Q_xQ_y + Q_xQ_z + Q_yQ_z), \tag{2}$$

TABLE II. Total energies (in mRy/unit cell) for the structures listed in Table I calculated with the PP method for two values of σ (in Ry). The total energy of the initial $P0$ phase is taken as the reference energy.

Smearing, σ	$P1$	$P2$	$P3$	$C1$	$C2$	$S1$
0.01	−9.865	−11.376	−10.569	−11.355	−10.493	−11.315
0.08	−0.088	−0.031	−0.088	−0.027	−0.119	−0.116

$$F(\mathbf{e}) = 1/6(C_{11}+2C_{12})e_A^2 + 1/12(C_{11}-C_{12})e_{E1}^2 + 1/4(C_{11}-C_{12})e_{E2}^2 + 1/2C_{44}(\epsilon_{xy}^2+\epsilon_{yz}^2+\epsilon_{xz}^2). \quad (3)$$

The sign of the coefficients is such that $\alpha,\beta,\gamma>0$; $\alpha<0$ and $\beta,\gamma>0$ when the temperature is above or below the transition temperature T_c, respectively. C_{11}, C_{12}, and C_{44} are the elastic constants. Correspondingly, $e_A=\epsilon_{xx}+\epsilon_{yy}+\epsilon_{zz}$, $e_{E1}=2\epsilon_{zz}-\epsilon_{xx}-\epsilon_{yy}$, and $e_{E2}=\epsilon_{xx}-\epsilon_{yy}$.

The term $F(\mathbf{e},\mathbf{Q})$ can be constructed by taking into account the following expansion for the symmetric square of $X_{3'}$:

$$X_{3'} \times X_{3'} = X_1. \quad (4)$$

Since only e_A and e_{E1} transform according to the X_1 representation,[20] expansion (4) implies that the $X_{3'}$ mode can couple to these homogeneous strains. Then

$$F(\mathbf{e},\mathbf{Q}) = Ae_A(Q_x^2+Q_y^2+Q_z^2) + Be_{E1}(2Q_z^2-Q_x^2-Q_y^2). \quad (5)$$

Spontaneous elastic strains in the tetragonal phase follows from the equilibrium condition, $\partial F/\partial e=0$,

$$e_A = -3A(Q_x^2+Q_y^2+Q_z^2)/(C_{11}+2C_{12}), \quad (6)$$

$$e_{E1} = -6B(2Q_z^2-Q_x^2-Q_y^2)/(C_{11}-C_{12}). \quad (7)$$

In our case, the $P0$ to $C2$ transition occurs along the $C2$ direction and $Q_x=Q_1$, $Q_y=Q_1$, $Q_z=Q_2$, and spontaneous volume e_A and tetragonal e_{E1} elastic strains are expected to appear as follows:

$$e_A = -3A(Q_1^2+2Q_1^2)/(C_{11}+2C_{12}), \quad (8)$$

$$e_{E1} = -12B(Q_2^2-Q_1^2)/(C_{11}-C_{12}). \quad (9)$$

Therefore the spontaneous elastic strains, e_A and e_{E1}, are induced indirectly by the collapse of the $X_{3'}$ mode, which indicates that the tetragonal phase is improper ferroelastic.

One can easily show[23] that the coupling between the soft phonon and the macroscopic strain renormalizes the fourth-order coefficient in Eq. (2), making it large and negative, whenever $C_{11}+2C_{12}$ and $C_{11}-C_{12}$ are small. As a rule, the shear modulus $C_{11}-C_{12}$ softens at the transition temperature,[23] in which case the transition must then be first order. Another way of explaining this first-order transition is to consider the expansion of the free energy up to sixth order in the order parameter and to fit the coefficients to first-principles calculations. However, to do this in practice is very difficult because of the existence of high-order invariants and small energy differences. Instead we preferred to focus on the geometrical optimization of several possible structures that can arise as a result of the collapse of the acoustic $X_{3'}$ mode. We performed full-energy minimizations with respect to atomic displacements, strain parameters, and cell volume for the seven structures listed in Table I as functions of the smearing parameter σ. The total energies for these possible structures calculated for two boundary values $\sigma=0.01$ and 0.08 Ry are summarized in Table II. It is clearly seen that all these phases are more stable than the initial cubic structure. However, at high σ the favored phase is $C2$, whereas at low σ the $P2$ phase is the most stable. Below we will re-examine these latter structures. To simplify the structural analysis we will consider these phases in terms of atomic displacements $X_{\mathrm{V,N}}$ and $Z_{\mathrm{V,N}}$ in the crystal coordinates,

$$\mathrm{V}(X_\mathrm{V},X_\mathrm{V},Z_\mathrm{V}),\quad \mathrm{V}(1/2-X_\mathrm{V},1/2-X_\mathrm{V},Z_\mathrm{V}),$$

$$\mathrm{V}(1/2-X_\mathrm{V},X_\mathrm{V},1/2-Z_\mathrm{V}),\quad \mathrm{V}(X_\mathrm{V},1/2-X_\mathrm{V},1/2-Z_\mathrm{V}),$$

$$\mathrm{N}(1/2+X_\mathrm{N},1/2+X_\mathrm{N},1/2+Z_\mathrm{N}),\quad \mathrm{N}(1/2+X_\mathrm{N},-X_\mathrm{N},-Z_\mathrm{N}),$$

$$\mathrm{N}(-X_\mathrm{N},1/2+X_\mathrm{N},-Z_\mathrm{N}),\quad \mathrm{N}(-X_\mathrm{N},-X_\mathrm{N},1/2+Z_\mathrm{N}). \quad (10)$$

Before we proceed with the detailed analysis of these phases, let us compare the results of the calculations of the $P0$, $P2$, and $C2$ structures by both methods, PP and FLAPW, to check the reliability of the conditions that were selected for the PP calculations. The results obtained by both methods are presented in Table III. The FLAPW method gives larger c/a ratios and atomic displacements than those obtained with the PP approach. As for the rest, both approaches give similar results, which show that our PP calculations were carried out with acceptable accuracy.

The study of structural stability of a crystal should begin from an analysis of the Gibbs free energy that is given in our case by

$$G = E_T + F_{\mathrm{vib}} + F_{\mathrm{conf}}, \quad (11)$$

where E_T is the ground-state energy obtained from DFT total-energy calculations, F_{vib} represents the vibrational contribution to the total free energy, and the third term, F_{conf}, is the configuration part of the total free-energy G. Since we assume that the phase transition in VN_x is caused by an electronic instability, we will concentrate in the following on an analysis of the first term of expression (11), neglecting the vibrational and configurational contributions to the free energy.

In Fig. 6 we show the total energy, cell volume, frequencies of soft modes, and structural characteristics of the $C2$ and $P2$ phases as functions of the smearing parameter σ. The

TABLE III. Lattice parameter (a), c/a ratio, and total energy of the initial cubic phase (E_T) and atomic displacements $X_{V,N}$ and $Z_{V,N}$ for the $C2$ and $P2$ structures [cf. Eq. (10)], computed with the PP (σ =0.01 Ry) and FLAPW methods. The PP, FLAPW, and experimental (Ref. 7) lattice constants for the $P0$ phase are 4.118, 4.132 and 4.133 Å, respectively.

Structure	Method	a (Å)	c/a	ΔE_T (mRy)	X_V	Z_V	X_N	Z_N
$C2$	PP	4.121	0.9981	10.493	0.0184	0.0171	0.0099	0.0092
	FLAPW	4.135	0.9977	5.983	0.0220	0.0194	0.0111	0.0097
$P2$	PP	4.151	0.9772	11.376	0.0223		0.0114	
	FLAPW	4.175	0.9719	9.512	0.0248		0.0120	

results indicate that the $P0$ to $C2$ phase transition takes place below σ=0.07–0.08 Ry. Since, for σ=0.08 Ry, the total-energy difference between the two structures $E_T \sim 0.1$ mRy is comparable to the accuracy of the PP calculations, the onset of the phase transition should be assigned to σ =0.07 Ry (E_T=0.5 mRy). The onset of phonon softening falling on σ=0.07 Ry speaks also in favor of this association [cf. Fig. 6(b)]. With a further decrease in σ the $C2$ structure transforms into the $P2$ one, indicating that the $C2$ structure is not stable at low σ (or temperature) in agreement with

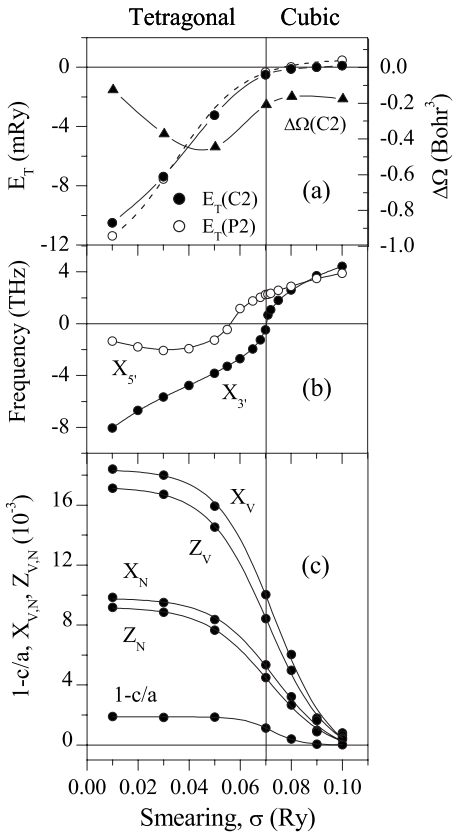

FIG. 6. Total energies (E_T) of the $P2$ and $C2$ phases, relative to the total energy of the $P0$ phase, (a) differences between cell volumes $\Delta\Omega=\Omega(C2)-\Omega(P0)$, (b) frequencies of the $X_{3'}$ and $X_{5'}$ acoustic phonons in the $P0$ phase, and (c) structural parameters [cf. Eq. (10)] for the $C2$ phase as functions of σ. The vertical line defines as a function of two subregions in which the tetragonal and cubic structures are stable.

experiment.[7] In accordance with the XRD measurements,[7] the low-temperature phase has a triclinic structure close to the tetragonal one. An additional structural optimization of the triclinic phase was performed, and it was found that the total energy was higher than that of the $P2$ phase (by 0.3 mRy). Therefore, we conclude that the low-temperature phase could be correctly described only if the configuration term in Eq. (11) was taken into account.

Coming back to Fig. 6 we note that, for each value of σ, the cell volume of the tetragonal phase is less than that of the cubic structure. This means that at the transition point (σ $\sim$0.07 Ry) the volume will change abruptly, indicating that the $P0$ to $C2$ phase transition is first order. We see from Fig. 6(b) that the $X_{3'}$ acoustic phonon abruptly softens at the transition point, whereas the frequency of the $X_{5'}$ acoustic phonon becomes soft at lower σ, indicating that it is the $X_{3'}$ acoustic-phonon softening that is responsible for the phase transition.

Figure 6(c) shows the gradual increase in the $1-c/a$ ratio and the atomic displacements for the $C2$ phase with a decrease in σ. An increase in these characteristics leads to a lowering of the total energy and to a stabilization of the $C2$ phase at and below the transition point ($\sigma \sim 0.07$ Ry) [$E_T(C2) < E_T(P0)$; cf. Fig. 6(a)]. Above the transition point only the cubic phase is stable, i.e., the $1-c/a$ ratio and the atomic displacements tend toward zero. Thus the $1-c/a$ ratio and the atomic displacements $X_{V,N}$ and $Z_{V,N}$ change abruptly at the transition point, which suggests a first-order phase transition.

The mechanism of the phase transition in vanadium nitride described above predicts the phonon softening at the transition point $\sigma \sim 0.07$ Ry. The stabilization of the cubic structure occurs above 205 K and at a negligible deviation from stoichiometry (Δx=0.03).[7] This implies that the structures calculated at $\sigma \sim 0.075$–0.08 Ry will correspond to the almost stoichiometric compositions: a small reduction in σ will cause the phonon softening. The results presented in Fig. 3 speak in favor of this conclusion. Indeed, an excellent agreement between the calculated and experimental PDOSs for the stoichiometric VN was achieved for σ $\sim$0.09–0.10 Ry. This suggests that the stoichiometric vanadium nitride has a considerable number of vacancies in both sublattices.[8]

In Table IV we present the theoretical and experimental structural parameters for the $C2$ phase. One can see that the crystalline structure predicted by our calculations is very close to that experimentally observed.[7]

TABLE IV. Comparison between the calculated (PP) and experimental (XRD) structural characteristics for the $C2$ phases. Notation: a,c-lattice parameters, $\Delta\Omega$ difference between the cell volumes of the $C2$ and $P0$ structures, and $X_{V,N}$ and $Z_{V,N}$ the atomic displacements [cf. Eq. (10)].

Method	a (Å)	c/a	$\Delta\Omega$ (Å^3)	X_V	Z_V	X_N	Z_N
PP(σ=0.07 Ry)	4.138	0.9989	0.03	0.0100	0.0084	0.0053	0.0045
PP(σ=0.08 Ry)	4.141	0.9996	0.02	0.0061	0.0050	0.0032	0.0027
XRD[a]	4.127	0.9992	<0.1	0.0057	0.0052	0.0035	0.0033

[a]Experimental results (Ref. 7).

It follows from our model that the phonon anomalies in the cubic phase and the thermal displacement of the metal atoms caused by the softening of the X_3' acoustic phonon are responsible for an increase in the $\langle u^2\rangle_V/\langle u^2\rangle_N$ ratio with a temperature decrease, in agreement with experiment. Since atomic displacements forego the tetragonal distortion, we conclude that phonon collapse can be accompanied by the appearance of a peak in the temperature dependence of the heat capacity.[7] Here it should be noted that a similar feature of a first-order phase transition was observed in the case of CrN.[24] As for substoichiomentric VN_x, a lowering of the Fermi level, relative the W_3' level with a decrease in x, leads to an increase in the frequencies of soft phonons. As a result, the nitrogen vacancies stabilize the cubic structure. Thus, we see that the suggested model of the structural transformation in VN_x correctly describes almost all the observations mentioned in Sec. I except for the existence of the low-temperature triclinic phase. To successfully predict such a phase, along with the total-energy contribution, the configurational contribution to the free energy should be taken into account. In conclusion, we note that our study of the phase transition in VN_x has a semiquantitative character since we correlate in a phenomenological way the smearing parameter σ to temperature and vacancy composition: "an increase in σ implies a corresponding increase in temperature or vacancy composition." Nevertheless, such an approach that is based on an analysis of the total energies of various structures as functions of σ enabled us to rather correctly describe the main features of the complex phase transition in vanadium nitride.

IV. CONCLUSIONS

In this paper we have shown that an approach based on the Landau theory of phase transitions coupled to accurate first-principles calculations of the electronic structure and phonon properties enabled us to propose a plausible mechanism for the cubic $Fm\bar{3}m$ to tetragonal $P\bar{4}2m$ phase transition in VN_x at low temperatures. Soft X_3' and X_5' acoustic modes for the high-temperature cubic phase are predicted. It was shown earlier[8] that the phonon anomalies in VN originated from electronic transitions between W_3' states. We show that the elastic instability arises from a coupling between the soft X_3' acoustic mode and spontaneous volume and tetragonal strains, indicating that the tetragonal $P\bar{4}2m$ phase is improper ferroelastic. The quantitative analysis of the energetics of the possible structures confirms this model. The influence of temperature or nitrogen vacancies on the phase transition in VN_x is approximated by means of varying the band-energy smearing parameter, σ. It was shown that an increase in σ (that implies an increase in temperature or vacancy composition) shifts down the Fermi level, respective to the W_3' level, and causes a lattice expansion. As a result, the frequency of the soft mode increases and the cubic structure stabilizes. This finding is consistent with the results of the phonon spectrum calculations for the ordered substoichiometric $VN_{0.75}$ compound. An abrupt change in cell volume and structural parameters as functions of σ suggests a first-order transition. Since the structural transformation begins as a second-order phase transition owing to a softening of a X_3' mode, an anomaly in the temperature dependence of the heat capacity is expected. The calculated tetragonal phase agrees fairly well with the experimental low-temperature structure.

ACKNOWLEDGMENTS

This work was supported by National Academy of Science of Ukraine under Contracts No. III-35-07(C) and No. 86/08-H. The work of P.E.A.T. was performed under the auspices of the U.S. Department of Energy by Lawrence Livermore National Laboratory under Contract No. DE-AC52-07NA27344.

[1] L. E. Tot, *Transition Metal Carbides and Nitrides* (Academic, New York, 1971).

[2] V. A. Gubanov, A. L. Ivanovsky, and V. Zhukov, *Electronic Structure of Refractory Carbides and Nitrides* (Cambridge University Press, Cambridge, 1994).

[3] A. Neckel, P. Rastl, R. Eibler, P. Weinberger, and K. Schwarz, J. Phys. C **9**, 579 (1976).

[4] P. Marksteiner, P. Weinberger, A. Neckel, R. Zeller, and P. H. Dederichs, Phys. Rev. B **33**, 812 (1986).

[5] T. Onozuka, J. Appl. Crystallogr. **11**, 132 (1978).

[6] E. I. Isaev, S. I. Simak, I. A. Abrikosov, R. Ahuja, Y. K. Vekilov, M. I. Katsnelson, A. I. Lichtenstein, and B. Johansson, J. Appl. Phys. **101**, 123519 (2007).
[7] F. Kubel, W. Lengauer, K. Yvon, K. Knorr, and A. Junod, Phys. Rev. B **38**, 12908 (1988).
[8] W. Weber, P. Roedhammer, L. Pintschovius, W. Reichardt, F. Gompf, and A. N. Christensen, Phys. Rev. Lett. **43**, 868 (1979).
[9] S. Baroni *et al.*, http://www.pwscf.org/, 1995.
[10] D. Vanderbilt, Phys. Rev. B **41**, 7892 (1990).
[11] J. P. Perdew, K. Burke, and M. Ernzerhof, Phys. Rev. Lett. **77**, 3865 (1996).
[12] H. J. Monkhorst and J. D. Pack, Phys. Rev. B **13**, 5188 (1976).
[13] D. Vanderbilt and S. G. Louie, Phys. Rev. B **30**, 6118 (1984).
[14] S. Baroni, S. D. Gironcoli, A. D. Corso, and P. Gianozzii, Rev. Mod. Phys. **73**, 515 (2001).
[15] W. Frank, C. Elsasser, and M. Fahnle, Phys. Rev. Lett. **74**, 1791 (1995).
[16] D. Alfe, http://chianti.geol.ucl.ac.uk/dario, 1998.
[17] P. Blaha, K. Schwarz, P. Sorantin, and S. B. Trickey, Comput. Phys. Commun. **59**, 399 (1990).
[18] P. Blaha, K. Schwarz, and J. Luitz, WIEN97, Vienna University of Technology, Wien, 1997.
[19] J. S. Kim, D. M. Hatch, and H. T. Stokes, Phys. Rev. B **33**, 1774 (1986).
[20] H. T. Stokes, D. M. Hatch, and B. J. Campbell, ISOTROPY, 2007, (http://stokes.byu.edu/isotropy.html).
[21] L. D. Landau and E. M. Lifshitz, *Statistical Physics* (Pergamon, Oxford, 1980).
[22] K. Negita, Acta Metall. **37**, 313 (1989).
[23] M. Buongiorno Nardelli, S. Baroni, and P. Giannozzi, Phys. Rev. B **51**, 8060 (1995).
[24] J. D. Browne, P. R. Liddell, R. Street, and T. Mills, Phys. Status Solidi A **1**, 715 (1970).